Article
Vol. 23, No. 3, p. 489–507, June 2019
https://doi.org/10.1007/s12303-018-0058-4
pISSN 1226-4806 eISSN 1598-7477
Geosciences Journal GJ

Identification of sedimentary-diagenetic facies and implications for reservoir quality: evidence from the Eocene coarse-grained deposits in the Dongying Depression, Bohai Bay Basin, China

Yanzhong Wang[1]*, Yingchang Cao[1], Benben Ma[2], Kelai Xi[1], Xin Cheng[1], and Mingshui Song[3]

[1]School of Geosciences, China University of Petroleum, Qingdao 266580, China
[2]Key Laboratory of Tectonics and Petroleum Resources (China University of Geosciences), Ministry of Education, Wuhan 430074, China
[3]Shengli Oilfield Company, SINOPEC, Dongying, Shandong 257015, China

ABSTRACT: Facies identification is a fundamental issue on evaluation and prediction for siliciclastic sediments. The purpose of this paper is to identify sedimentary-diagenetic facies and investigate the influence of sedimentary-diagenetic facies on reservoir quality in coarse-grained deposits from the Eocene Es4 interval, Dongying Depression, Bohai Bay Basin. Based on detailed core observation, thin section petrography combined with conventional wireline logs and core measurement analysis, 12 types of sedimentary-diagenetic facies were divided according to their lithofacies, diagenetic products and related contributions to reservoir quality. The identification and spatial distribution of these sedimentary-diagenetic facies can be determined based on the Bayes discriminant analysis and related cross-plot analysis. The variations of porosity and permeability with burial depth were precisely determined with ±2% for porosity and $\pm 1 \times 10^{-3}$ μm^2 for permeability. The spatial distribution of reservoir porosity and permeability can be predicted quantitatively: high zones of porosity and permeability mainly distributed in the central sections of thick-bedded sandbody, ranging from 6% to greater than 12% for reservoir porosity and from 1×10^{-3} μm^2 to greater than 6×10^{-3} μm^2; relatively low zones of porosity (less than 6%) and permeability (less than 1×10^{-3} μm^2) mainly occur in the bottom and the margin of the thick-bedded sandbody.

Key words: sedimentary-diagenetic facies, wireline logs, coarse-grained deposits, Eocene, Bohai Bay Basin

Manuscript received January 27, 2018; Manuscript accepted July 8, 2018

1. INTRODUCTION

Facies identification exerts a significant influence on oil exploration and development and is also the basis of reservoir quality evaluation (Li and Anderson-Sprecher, 2006; He et al., 2016; Cui et al., 2017). Identification of facies involves with two important aspects: lithofacies and diagenetic facies identification. Lithofacies refers to initial rock or rock association deposited under certain sedimentary environments and significantly affects original reservoir quality and architecture (Bjørlykke, 2014; He et al., 2016; Lai et al., 2017). Diagenetic facies, mainly inherited by initial lithofacies, is associated with types and degree of diagenetic products exerted by mechanical compaction, mineral cementation and dissolution, and can greatly influences the evolution of reservoir quality (Zou et al., 2008; Lai et al., 2016; Cui et al., 2017). As the identification of facies is critically constrained by limited amounts of core and outcrop data, therefore, wireline logs are the alternative options which are widely used to determine the lithofacies and diagenetic facies of various depositional systems based on their specific log responses (Xu et al., 2009; Ozkan et al., 2011; Cui et al., 2017). The present-day statistical methods of facies identification associated with conventional wireline logs mainly consist of discriminant analysis, clustering analysis, cross plotting, fuzzy diagnosis, and Artificial Neural Network (ANN) (Li and Anderson-Sprecher, 2006; He et al., 2016; Cui et al., 2017). However, these identification methods related to wireline logging in different depositional environments are only focused on lithofacies or diagenetic facies separately in previous studies (e.g., Ozkan et al., 2011; Lai et al., 2016; Cai et al., 2017). Actually, the wireline log responses of

*Corresponding author:
Yanzhong Wang
School of Geosciences, China University of Petroleum, Qingdao 266580, China
Tel: +86-18253266698, E-mail: wangyanzhong1980@163.com

different reservoir architectures in burial environment are influenced by combined effects of initial lithofacies and later diagenetic facies, especially for the coarse-grained sediments in deep burial environment. In this study, we propose "sedimentary-diagenetic facies" concept which integrates lithofacies and associated diagenetic facies together in specific burial environment. The evaluation of reservoir quality associated with lack of core and outcrop data can be directly determined by continuous identification of sedimentary-diagenetic facies based on conventional wireline logs. The integrated identification of sedimentary-diagenetic facies can greatly enhance predictive models of reservoirs and has potential application for various deposition systems in similar sedimentary-tectonic settings.

This study focuses on coarse-grained sediments deposited in a sublacustrine-fan setting in the Eocene Es4 interval at burial depths of 2500–4000 m in the Dongying Depression, Bohai Bay Basin in eastern China (Fig. 1a). Lithofacies of the Es4 interval varies greatly and mainly includes coarse-grained conglomerates, pebbly sandstones, sandstones, and lacustrine mudstones (Ma et al., 2017). Diagentic products in the Eocene Es4 interval mainly consist of strong mechanical compaction, precipitation of predominated carbonate minerals and other minor phases of authigenic quartz and clay minerals (Wang et al., 2014; Ma et al., 2016). In this study, we established a new concept model "sedimentary-diagenetic facies" for facies identification based on conventional wireline logs and evaluated related reservoir quality of sublacustrine fan in the Eocene Es4 interval in the Dongying Depression. Thus, the objectives of this study are to: (1) illustrate the features of lithofacies and corresponding diagenetic facies and summary the characteristics of sedimentary-diagenetic facies based on core observation and thin section petrography; (2) identify sedimentary-diagenetic facies based on conventional wireline logs; and (3) determine the influence of sedimentary-diagenetic facies on reservoir quality and evaluate the distribution of high-quality reservoir.

2. GEOLOGICAL SETTING

The Dongying Depression is a sub-tectonic unit and is located at southern part of Jiyang Subbasin, Bohai Bay Basin. The Dongying Depression, covering an area of 5850 km^2, is bounded to the east by the Qingtuozi Uplift, to the south by the Luxi Uplift and Guangrao Uplift, to the west by the Qingcheng Uplift, and to the north by the Chenjiazhuang and Qingtuozi Uplift (Fig. 1b). The Minfeng Sag is located in the northeastern part of the Dongying Depression and the northern margin of the sag is confined by the Chennan Boundary Fault (Fig. 1c; Jiang et al., 2013).

Sedimentary sequences in the Dongying Depression, in ascending order, consist of the Paleogene Kongdian (Ek), Shahejie (Es), and Dongying (Ed) formations, the Neogene Guantao (Ng) and Minghuazhen (Nm) formations, and the Quaternary Pingyuan (Qp) Formation (Ma et al., 2017). The Eocene Es4 interval in the Dongying Depression is mainly characterized by dark lacustrine source rocks, calcareous mudstones interbedded with multi-stage, sublacustrine-fan, sandy conglomerates, pebbly sandstones and sandstones (Ma et al., 2017). During the deposition of the Es4 interval, terrigenous siliciclastic sediments were transported into the lake by gravity flows during duration of seasonal floods and large-scale sediments of sublacustrine fans were formed close to the footwall of the Chennan Boundary Fault and interfingered with more distal deep-lake mudstones.

3. SAMPLES AND METHODS

3.1. Well Logs

Based on log response characteristics of lithofacies from 15 boreholes, 5 sensitive log curves were selected for facies identification and include bulk density (DEN), compensated neutron log (CNL), sonic transit time (AC), natural gamma ray (GR), deep lateral log (RLLD) (Table 1). The matching of core with log curve was accomplished by correlating the CNL curve with core plug porosity. In addition, siliciclastic rocks in the Eocene Es4 interval are mainly derived from Archaean granitic gneiss which are enriched in alkali feldspar and mica minerals (Li and Zhou, 2008; Lu, 2010), therefore, the coarse-grained rocks (e.g., conglomerate, pebbly sandstone, sandstone) have higher contents of potassium than fine-grained rocks (e.g., mudstones, shales). This results in highest values of GR curve in coarse-grained rocks and lowest values of GR in fine-grained rocks (Table 1). In addition, the Bayes discriminant analysis of combined wireline logs was conducted by using the Statistical Product and Service Solutions (SPSS) software.

3.2. Rock Petrography

18 boreholes were observed and described in detail to determine rock lithologies, sedimentary structures and sediment body thicknesses. 95 representative core samples from 15 boreholes were thin sectioned, impregnated with red epoxy resin under vacuum and stained with alizarin red-S and potassium ferricyanide (Dickson, 1965), and then examined using a standard petrographic microscope. 400 point counts per thin section were conducted in order to determine compositions of detrital grains, authigenic minerals, intergranular volume and total porosities. 40 gold-coated sample chips were examined using a JSM-5500LV scanning electron microscope (SEM) to investigate authigenic minerals and

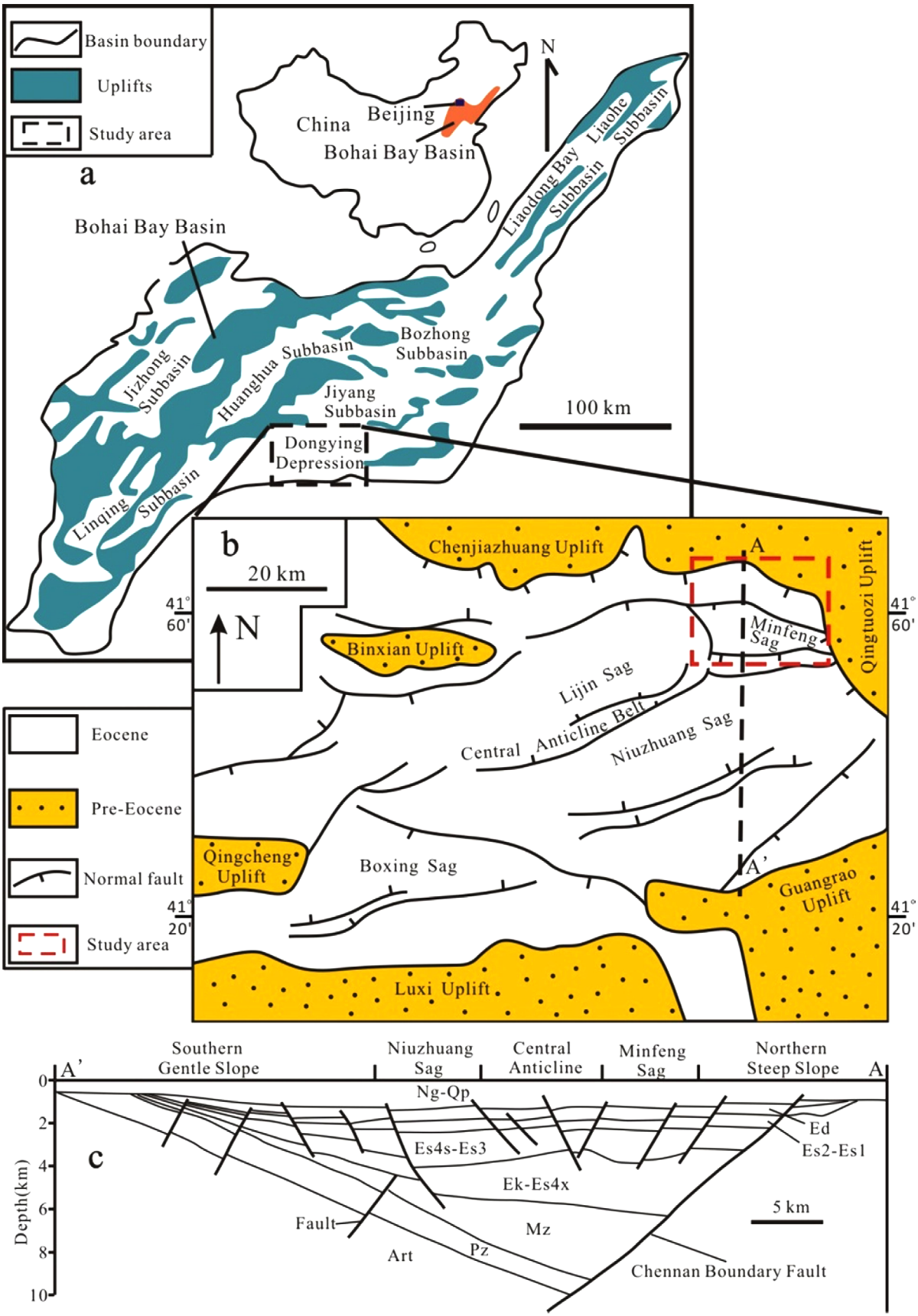

Fig. 1. (a) Locality map of subbasins of the Bohai Bay Basin, eastern China; (b) Distribution of main sags and uplifts and major faults and location of section A–A'; (c) Cross section A–A' showing major stratigraphic units and major tectonic features within the Dongying Depression.

https://doi.org/10.1007/s12303-018-0058-4

Table 1. Sensitive analysis of wireline logs for facies identification in the Eocene Es4 interval

Wireline log	Mudstone	Sandstone	Pebbly sandstone	Conglomerate
GR (API)	Relatively low value 70–125	Relatively high value 100–140	Relatively high value 102–165	High value 104–176
AC (μs/ft)	High value 62–90	Medium-low value 60–86	Medium-low value 58–84	Low value 54–72
DEN (g/cm^3)	Medium-low value 2.3–2.64	Medium-low value 2.48–2.66	Medium-low value 2.48–2.66	High value 2.48–2.66
CNL (%)	High value 6.0–26.0	Medium-low value 5.0–22.0	Medium-low value 5.0–14.0	Low value 2.0–10.0
RD (Ω.m)	Relatively low value 5–45	Relatively low value 10–50	Relatively high value 10–65	Relatively high value 10–75

pore types under an acceleration voltage of 20 kV using a beam current of 1.0–1.5 nA.

3.3. Core Porosity and Permeability

A total of 505 cylindrical core samples (diameter = 25 mm, length = 30–40 mm) from 16 boreholes were selected to determine core porosity and permeability at the Exploration and Development Research Institute of the Sinopec Zhongyuan Oilfield Company. The gas expansion method was used for determining porosity and helium was used as the measuring medium. Permeability was measured in a gas-autoclave using the pressure-transient technique (Rahman and McCann, 2012) and nitrogen was used as the permeating medium.

4. RESULTS

4.1. Rock Petrology

Based on point count data, most sandstones in the Es4 interval are coarse-grained and moderately to poorly sorted lithic arkoses and feldspathic litharenites based on ternary plot of Folk (1974), with the average compositions of framework grains being $Q_{30}F_{39}R_{31}$. Diagenetic products in Es4 interval include strong compaction, predominant carbonate minerals, subordinate quartz cements and minor authigenic clay minerals (Fig. 2). Thin section and SEM images show that pervasive dissolution of minerals occurred in most samples in Es4 interval, which were predominated by feldspar dissolution and minor carbonate mineral dissolution (Fig. 2).

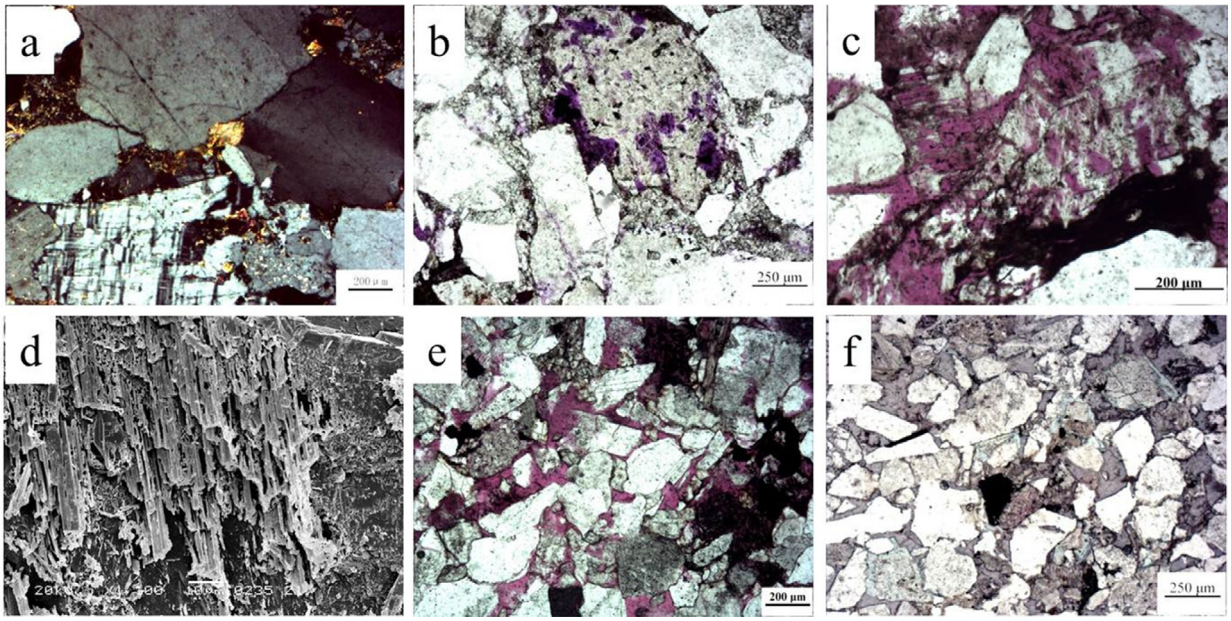

Fig. 2. Types and characteristics of diagenetic facies in the Eocene Es4 interval. (a) Strong compaction-weak cementation-weak dissolution diagenetic facies, Well Yan227, 3759.4 m; (b) Strong compaction-medium cementation-weak dissolution diagenetic facies, Well Yan23, 3674.95 m; (c) Medium compaction-weak cementation-strong dissolution diagenetic facies, Well Yong921, 2798.49 m; (d) Medium compaction-weak cementation-strong dissolution diagenetic facies, Well Yong92, 2971.92 m; (e) Medium compaction-weak cementation-medium dissolution diagenetic facies, Well Yan22-22, 3431.5 m; (f) Medium compaction-strong cementation-weak dissolution diagenetic facies, Well Yan22-22, 3350.25 m.

4.2. Sedimentary Lithofacies

Based on detailed core observation and description, 6 types of lithofacies are identified based on their sedimentary structures, sedimentary textures and bed thicknesses (Table 2), and includes matrix-supported conglomerate (Fig. 3a), grain-supported conglomerate (Fig. 3b), pebble-dominated sandstone (Fig. 3c), pebbly sandstone (Fig. 3d), sandstone (Fig. 3e) and mudstone (Fig. 3f).

4.3. Diagenetic Facies

Currently, quantitative classification methods of diagenetic facies are widely used to determine different types and degrees

Table 2. Description of different lithofacies in the Eocene Es4 interval

Lithofacies	Sedimentary structure	Sedimentary texture	Bed thickness	Rock color	Subfacies
Matrix-supported conglomerate	Massive bedding	Angular and subangular pebbles, poor sorted, coarse gravel predomominated and content of mud matrix more than 20%	2.5–30 m	Light gray–gray	Inner fan
Grain-supported conglomerate	Massive bedding	Subangular and sub-rounded pebbles, pebbles diameter mostly more than 10mm, sand matrix, poor sorted	0.5–30 m	Light gray–gray	Inner fan
Pebble-dominated sandstone	Massive or normal graded bedding	Subangular and sub-rounded pebbles, pebbles diameter mostly between 2~10 mm, pebbles content between 25~50%, grain-supported, relatively poor sorted	0.2–5 m	Light gray–gray	Middle fan
Pebbly sandstone	Massive or normal graded bedding	Subangular and sub-rounded pebbles, pebbles content between 10~25%, pebbles diameter mostly between 2~10 mm, relatively well sorted, grain-supported	0.15–4.5 m	Light gray–gray	Middle fan
Sandstone	Massive, normal graded or parallel bedding	Pebbles content less than 10%, relatively well sorted and rounded, mostly medium- to coarse-grained sand	0.05–2 m	Light gray–gray	Middle fan/ Outer fan
Mudstone	Massive or horizontally bedding	Extremely fine-grained and contain calcareous or pyrite concretions	0.02–0.35 m	Dark gray–black	Middle fan/ Outer fan

Fig. 3. Lithofacies types of coarse-grained sediments in the Eocene Es4 interval. (a) Matrix-supported conglomerate, Well Yan227, 3752.2 m; (b) Grain-supported conglomerate, Well Yan22-22, 3396.8 m; (c) Pebbly-dominated sandstone, Well Yong928, 3756.1 m; (d) Pebbly sandstone, Well Yan22-22, 3388.4 m; (e) Sandstone, Well Yong921, 2687.67 m; (f) Mudstone, Well Yan222, 4074.18 m.

https://doi.org/10.1007/s12303-018-0058-4

of diagenetic products in order to evaluate diagenetic effects on reservoir quality based on compaction rate (α), cementation rate (β) and dissolution rate (γ) (Liu et al., 2002; Zhang et al., 2009; Fu et al., 2013; Lai et al., 2015; Liu et al., 2015; Lai et al., 2016). These parameters can be expressed as below equations:

$$\alpha = (V_{priamry} - V_{cementation} + V_{dissolution})/V_{priamry} \times 100\%), \quad (1)$$

$$\beta = V_{cementation}/(V_{cementation} + V_{intergranular}) \times 100\%), \quad (2)$$

$$\gamma = V_{dissolution}/V_{present} \times 100\%. \quad (3)$$

$V_{primary}$ refers to primary pore volume; $V_{cementation}$ refers to pore volume of total cements; $V_{dissolution}$ refers to dissolution of total minerals; $V_{intergranular}$ refers to intergranular pore volume; $V_{present}$ refers to total present pore volume.

However, this classification method of diagenetic facies has several limitations: (1) the calculation equations for compaction rate, cementation rate and dissolution rate have different denominators which indicates these parameters do not have uniform standards and this will lead to unexpected discrepancy classification of diagenetic facies with the present reservoirs; (2) In some cases, there are no corresponding relationships between these parameters and their contributions to reservoir quality. For one case, if the reservoir was intensively compacted with very minor intergranular pores and these intergranular pores were totally filled with cements, then the intensively compacted reservoir would be classified as intensively cemented reservoir based on Equation (2). For another case, if the primary pores of the reservoir were completely destroyed by extensive compaction or cementation in the deep burial environment and only very minor dissolution pores occurred, then the extensive compacted or cemented reservoir would be wrongly classified as extensive dissolution reservoir based on Equation (3) (γ calculated as 100%).

The current classification method of diagenetic facies was not applicable for different types of reservoirs and will result in improper reservoir assessments. Therefore, we establish three new parameters ($P_{compaction}$, $P_{cementation}$ and $P_{dissolution}$) to quantitatively identify diagenetic facies and relate their corresponding contributions to the total reservoir quality. These parameters can be expressed as below equations:

$$P_{compaction} = P_{primary} + P_{dissolution} - P_{cementation} - P_{present}, \quad (4)$$

$$P_{cementation} = \text{two-dimension (2-D) cementation pore area} \times T, \quad (5)$$

$$P_{dissolution} = \text{2-D dissolution pore area} \times T. \quad (6)$$

$P_{compaction}$ refers to porosity loss related to mechanical compaction; $P_{cementation}$ refers to porosity loss related to mineral cementation; $P_{dissolution}$ refers to porosity increase related to mineral dissolution; $P_{primary}$ refers to total primary porosity; $P_{present}$ refers to present reservoir porosity. In addition, the two-dimension (2-D) cementation area includes the area which fills early-formed dissolution pores but does not contain the area that replaces particles.

Table 3. Classification standard for diagenetic facies related to mechanical compaction, cementation and dissolution in the Eocene Es4 interval

Intensity	$P_{compaction}$ (%)	$P_{cementation}$ (%)	$P_{dissolution}$ (%)
Strong	> 20	> 20	> 10
Medium	10–20	10–20	4–10
Weak	< 10	< 10	< 4

$P_{compaction}$ refers to porosity loss related to mechanical compaction; $P_{cementation}$ refers to porosity loss related to mineral cementation; $P_{dissolution}$ refers to porosity increase related to mineral dissolution.

T refers to the relationship between 2-D pore area and three-dimension (3-D) pore volume and can be expressed as below based on previous study in the Dongying Depression (Wang et al., 2013):

$$Y = 2.5203 \times X^{0.8457}. \quad (7)$$

Y refers to 3-D pore volume; X refers to 2-D pore area.

The primary porosity ($P_{primary}$) for different lithofacies can be estimated based on their corresponding sorting coefficient (So) in the previous studies in the Dongying Depression (Wang et al., 2013).

The siliciclastic reservoirs in the Eocene Es4 interval are buried from 2500 m to 4000 m and mainly experienced moderate to intensive compaction, multi-stage cementations and dissolutions. Based on the new classification method of diagenetic facies in this study, the resulting diagenetic facies can be determined according to classification standard (Table 3) and divided into five types including (Table 4): (1) strong compaction-weak cementation-weak dissolution diagenetic facies (Fig. 2a); (2) strong compaction-medium cementation-weak dissolution diagenetic facies (Fig. 2b); (3) medium compaction-weak cementation-strong dissolution diagenetic facies (Figs. 2c and d); (4) medium compaction-weak cementation-medium dissolution diagenetic facies (Fig. 2e); (5) medium compaction-strong cementation-weak dissolution diagenetic facies (Fig. 2f).

4.4. Types of Sedimentary-Diagenetic Facies

Based on detailed observations of cores and thin sections, not every lithofacies could produce various types of diagenetic facies during progressive burial. With initially bad sorting and immature compositions of framework grains, both matrix-supported conglomerate and grain-supported conglomerate lithofacies in the inner fan subfacies experienced strong compaction with extremely weak chemical diagenesis and only strong compaction-weak cementation-weak dissolution diagenetic facies developed for both lithofacies (Table 4). Pebbly-dominated

sandstones, pebbly sandstones and sandstones in the middle fan and outer fan subfacies have relatively well-sorted textures and mature compositions of framework grains (Table 2), and undergone different types and intensities of chemical diagenesis during progressive burial. This could result in strong compaction-weak cementation-weak dissolution diagenetic facies, medium compaction-strong cementation-weak dissolution diagenetic facies and medium compaction-weak cementation-strong dissolution diagenetic facies (Table 4). Compared with coarse-grained lithofacies, mudstones, the extremely fine-grained lithofacies, has unique sedimentary structures and textures, and therefore, are regarded as individual sedimentary-diagenetic facies. Therefore, twelve types of sedimentary-diagenetic facies are identified in the Eocene Es4 interval and include (Table 5): (1) strong compaction-medium cementation-weak dissolution matrix-supported conglomerate facies (Type 1); (2) strong compaction-medium cementation-weak dissolution grain-supported conglomerate facies (Type 2); (3) strong compaction-medium cementation-

Table 4. Classification results of diagenetic facies in the Eocene Es4 interval

Well	Depth (m)	$P_{primary}$ (%)	$P_{compaction}$ (%)	$P_{cementation}$ (%)	$P_{dissolution}$ (%)	$P_{present}$ (%)	Diagenetic facies
Yan22	3239.1	37	20.89	10.5	3.5	9.11	Strong compaction-medium cementation-weak dissolution
Yan22-22	3431.5	39.2	19.69	9.8	5.5	15.21	Medium compaction-weak cementation-medium dissolution
Yan22-22	3444.3	42.2	17.68	22.3	4.5	6.72	Medium compaction-strong cementation-weak dissolution
Yan22-22	3499.4	39.2	12.31	25	3	4.89	Medium compaction-strong cementation-weak dissolution
Yan22-22	3508.1	39.2	11.55	26.5	1.2	2.35	Medium compaction-strong cementation-weak dissolution
Yan22-22	3689.5	37	31.02	4.5	3.5	4.98	Strong compaction-weak cementation-weak dissolution
Yan23	3672.85	37	21.33	13.1	3.5	6.07	Strong compaction-medium cementation-weak dissolution
Yan23	3674.95	37	21.27	14.2	3.8	5.33	Strong compaction-medium cementation-weak dissolution
Yan222	4074.48	39.2	25.49	10.8	0.8	3.71	Strong compaction-medium cementation-weak dissolution
Yan222	4191.85	39.2	29.2	7.5	0	2.5	Strong compaction-weak cementation-weak dissolution
Yan227	3313.41	32	24.18	6.5	0	1.32	Strong compaction-weak cementation-weak dissolution
Yan227	3741.55	37	14.93	20.6	0	1.47	Medium compaction-strong cementation-weak dissolution
Yan 227	3759.4	37	26	4.5	0	6.5	Strong compaction-weak cementation-weak dissolution
YX21	3039.9	39.2	19.64	7.2	4.5	16.86	Medium compaction-weak cementation-medium dissolution
YX21	3053.65	42.2	17.68	7.5	6.5	23.52	Medium compaction- weak cementation- medium dissolution
YX21	3137.7	42.2	18.08	8.5	11.2	26.82	Medium compaction-weak cementation-strong dissolution
YX223	3738.7	35	21.8	9.5	0	3.7	Strong compaction-weak cementation-weak dissolution
Yong920	3585.2	35	22.1	7	0	5.9	Strong compaction-weak cementation-weak dissolution
Yong928	3907.3	39.2	31.13	5.5	1.1	3.67	Strong compaction-weak cementation-weak dissolution
Yong930	3994.8	35	20.69	11.5	0	2.81	Strong compaction-medium cementation-weak dissolution
F8	4055.75	35	26.01	5.1	0	3.89	Strong compaction-weak cementation-weak dissolution
FS1	3917	35	24.98	7.2	0	2.82	Strong compaction-weak cementation-weak dissolution
FS10	3915.35	39.2	22.57	13.9	0	2.73	Strong compaction-medium cementation-weak dissolution

https://doi.org/10.1007/s12303-018-0058-4

Table 5. Types and characteristics of sedimentary-diagenetic facies in the Eocene Es4 interval

Lithofacies (→)	Matrix-supported onglomerate	Grain-supported conglomerate	Pebbly-dominated sandstone	Pebbly sandstone	Sandstone	Mudstone
Diagenetic facies	Sedimentary-diagenetic facies					
Strong compaction-medium cementation-weak dissolution	Type 1	Type 2	Type 3	–	–	–
Strong compaction-weak cementation-weak dissolution	–	–	–	Type 6	Type 9	–
Medium compaction-strong cementation-weak dissolution	–	–	Type 4	Type 7	Type 10	–
Medium compaction-weak cementation-medium dissolution	–	–	Type 5	–	–	–
Medium compaction-weak cementation-strong dissolution	–	–	–	Type 8	Type 11	–

Type 1 = strong compaction-medium cementation-weak dissolution matrix-supported conglomerate facies; Type 2 = strong compaction-medium cementation-weak dissolution grain-supported conglomerate facies; Type 3 = strong compaction-medium cementation-weak dissolution pebbly-dominated sandstone facies; Type 4 = medium compaction-strong cementation-weak dissolution pebbly-dominated sandstone facies; Type 5 = medium compaction-weak cementation-medium dissolution pebbly-dominated sandstone facies; Type 6 = strong compaction-weak cementation-weak dissolution pebbly sandstone facies; Type 7 = medium compaction-strong cementation-weak dissolution pebbly sandstone facies; Type 8 = medium compaction-weak cementation-strong dissolution pebbly sandstone facies; Type 9 = strong compaction-weak cementation-weak dissolution sandstone facies; Type 10 = medium compaction-strong cementation-weak dissolution sandstone facies; Type 11 = medium compaction-weak cementation-strong dissolution sandstone facies; Type 12 = mudstone facies.

weak dissolution pebbly-dominated sandstone facies (Type 3); (4) medium compaction-strong cementation-weak dissolution pebbly-dominated sandstone facies (Type 4); (5) medium compaction-weak cementation-medium dissolution pebbly-dominated sandstone facies (Type 5); (6) strong compaction-weak cementation-weak dissolution pebbly sandstone facies (Type 6); (7) medium compaction-strong cementation-weak dissolution pebbly sandstone facies (Type 7); (8) medium compaction-weak cementation-strong dissolution pebbly sandstone facies (Type 8); (9) strong compaction-weak cementation-weak dissolution sandstone facies (Type 9); (10) medium compaction-strong cementation-weak dissolution sandstone facies (Type 10); (11) medium compaction-weak cementation-strong dissolution sandstone facies (Type 11); (12) mudstone facies (Type 12).

4.5. Reservoir Porosity and Permeability

Cross-plot of plug porosity and plug permeability of the Es4 reservoirs shows that reservoir porosity ranges from 1.0% to 21.2%, with an average of 9.3%, and reservoir permeability ranges from 0.003×10^{-3} μm^2 to 489.56×10^{-3} μm^2 with an average of 18.07×10^{-3} μm^2 (Fig. 4). The Es4 reservoirs show a relatively good correlation between porosity and permeability (Fig. 4).

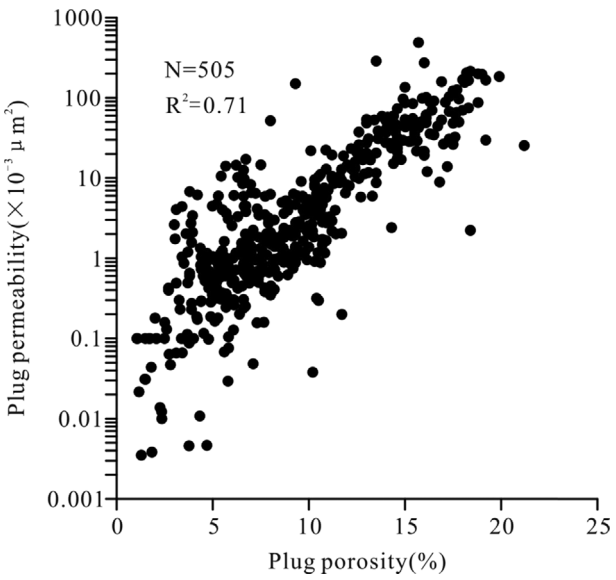

Fig. 4. Cross-plot of plug porosity versus plug permeability in the Eocene Es4 interval, showing a relatively good correlation between porosity and permeability (R^2 = 0.71).

5. DISCUSSION AND IMPLICATIONS

5.1. Wireline Log Identification of Sedimentary-Diagenetic Facies

As described above, the current identification methods of sedimentary lithofacies or diagenetic facies associated with wireline logs mainly consist of discriminant analysis (include Bayes and Fisher discriminant analysis), clustering analysis, cross plotting, fuzzy diagnosis, and Artificial Neural Network (Li and Anderson-Sprecher, 2006; He et al., 2016; Cui et al., 2017). However, a single facies identification method associated with wireline logs might result in some uncertainties or even errors, especially for the complex reservoirs in the deep burial environment (e.g., Li and Anderson-Sprecher, 2006). Based on log responses of each sedimentary-diagenetic facies in the Eocene Es4 interval (Fig. 5; Table 6), relatively significant differences occur among

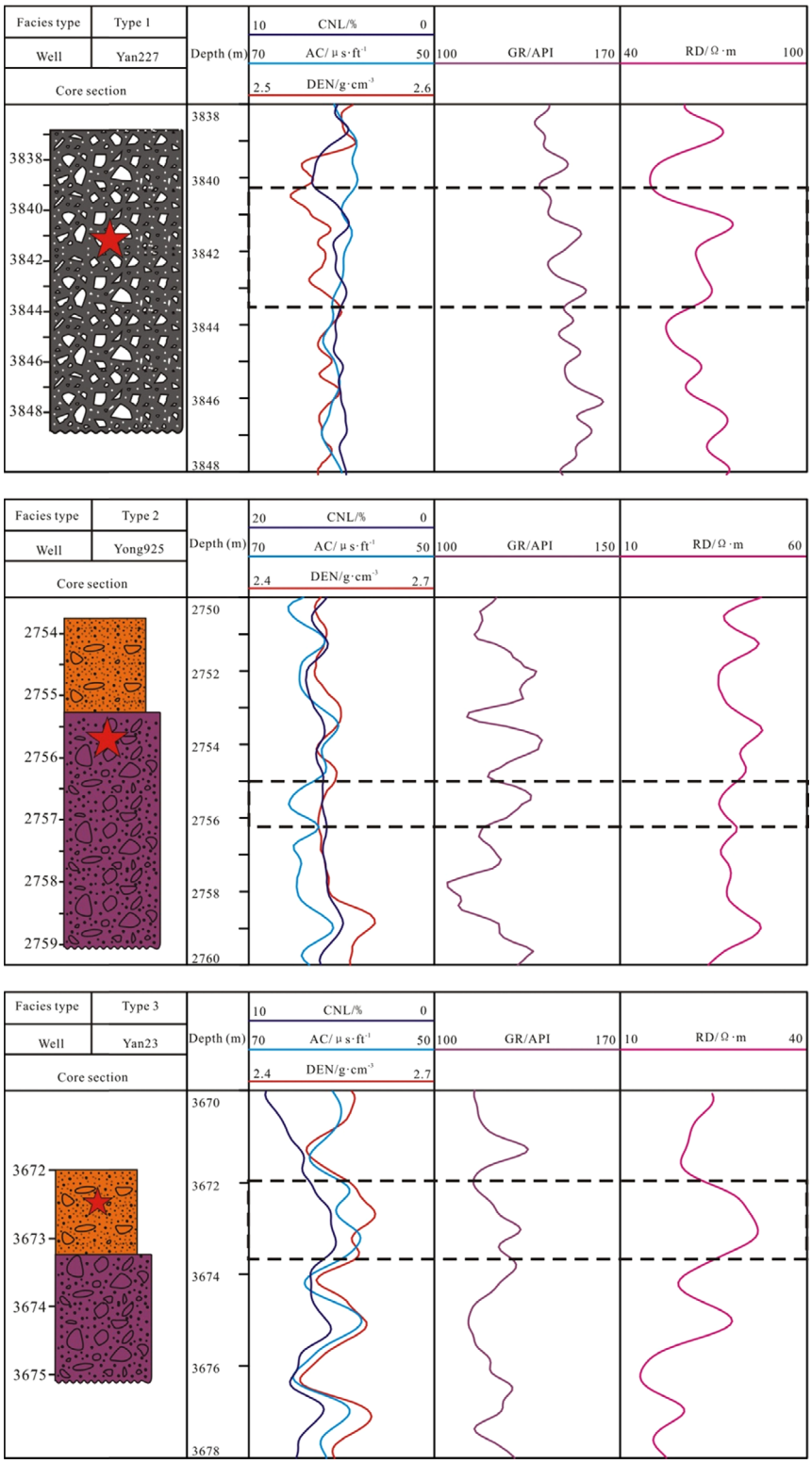

Fig. 5. Wireline log response of different sedimentary-diagenetic facies in the Eocene interval. Type 1 = strong compaction-medium cementation-weak dissolution matrix-supported conglomerate facies; Type 2 = strong compaction-medium cementation-weak dissolution grain-supported conglomerate facies; Type 3 = strong compaction-medium cementation-weak dissolution pebbly-dominated sandstone facies; Type 4 = medium compaction-strong cementation-weak dissolution pebbly-dominated sandstone facies; Type 5 = medium compaction-weak cementation-medium dissolution pebbly-dominated sandstone facies; Type 6 = strong compaction-weak cementation-weak dissolution pebbly sandstone facies; Type 7 = medium compaction-strong cementation-weak dissolution pebbly sandstone facies; Type 8 = medium compaction-weak cementation-strong dissolution pebbly sandstone facies; Type 9 = strong compaction-weak cementation-weak dissolution sandstone facies; Type 10 = medium compaction-strong cementation-weak dissolution sandstone facies; Type 11 = medium compaction-weak cementation-strong dissolution sandstone facies; Type 12 = mudstone facies.

https://doi.org/10.1007/s12303-018-0058-4

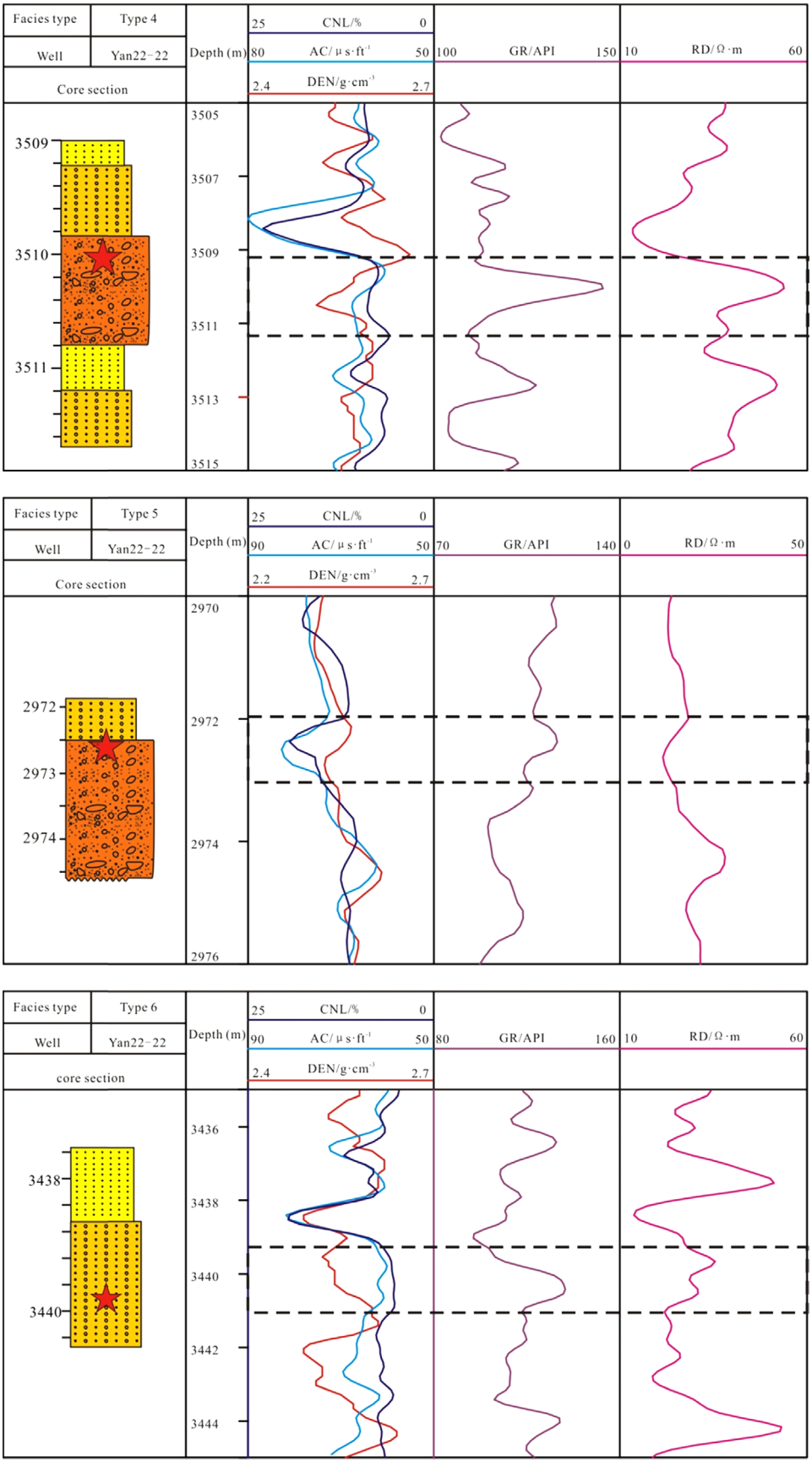

Fig. 5. (continued).

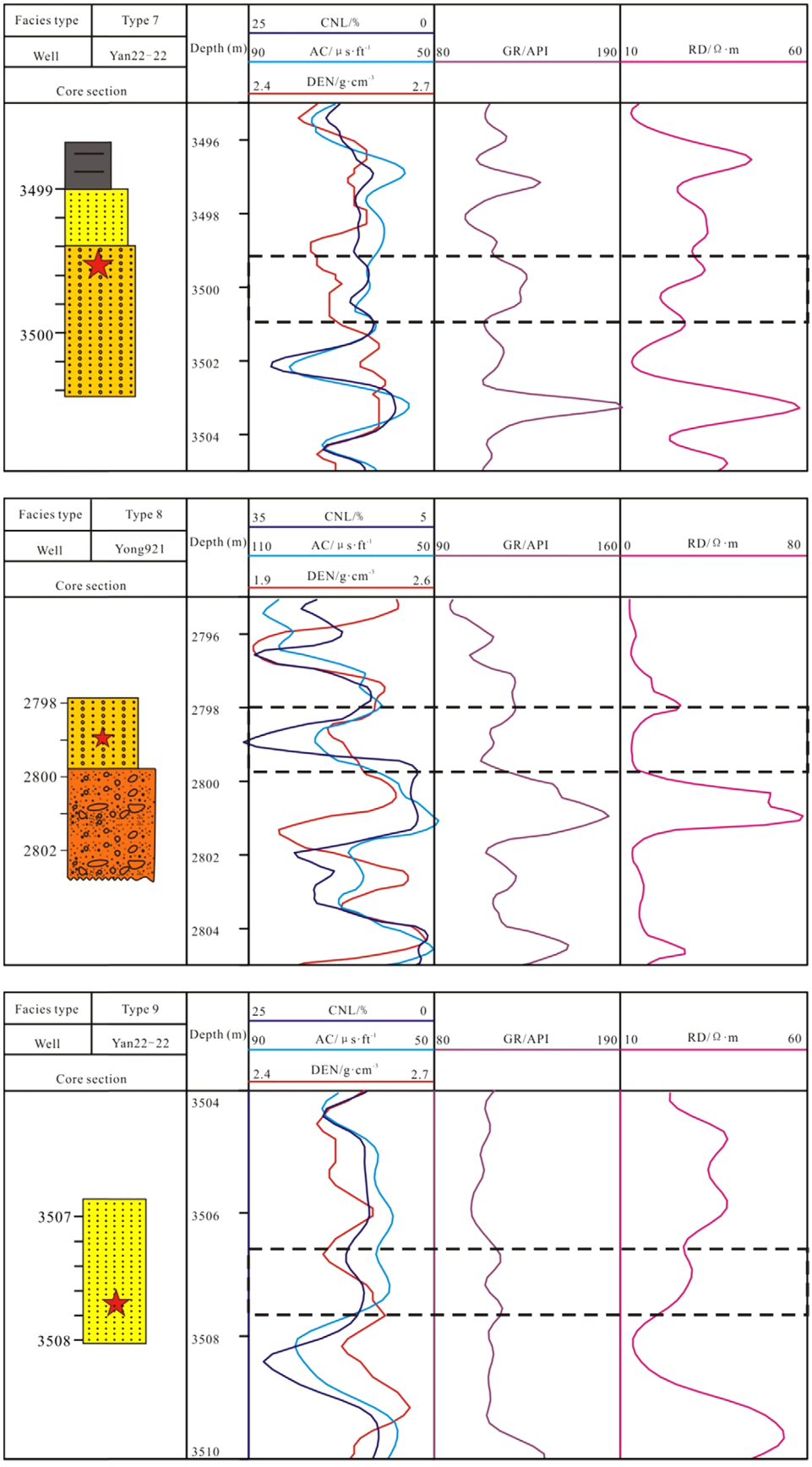

Fig. 5. (continued).

https://doi.org/10.1007/s12303-018-0058-4

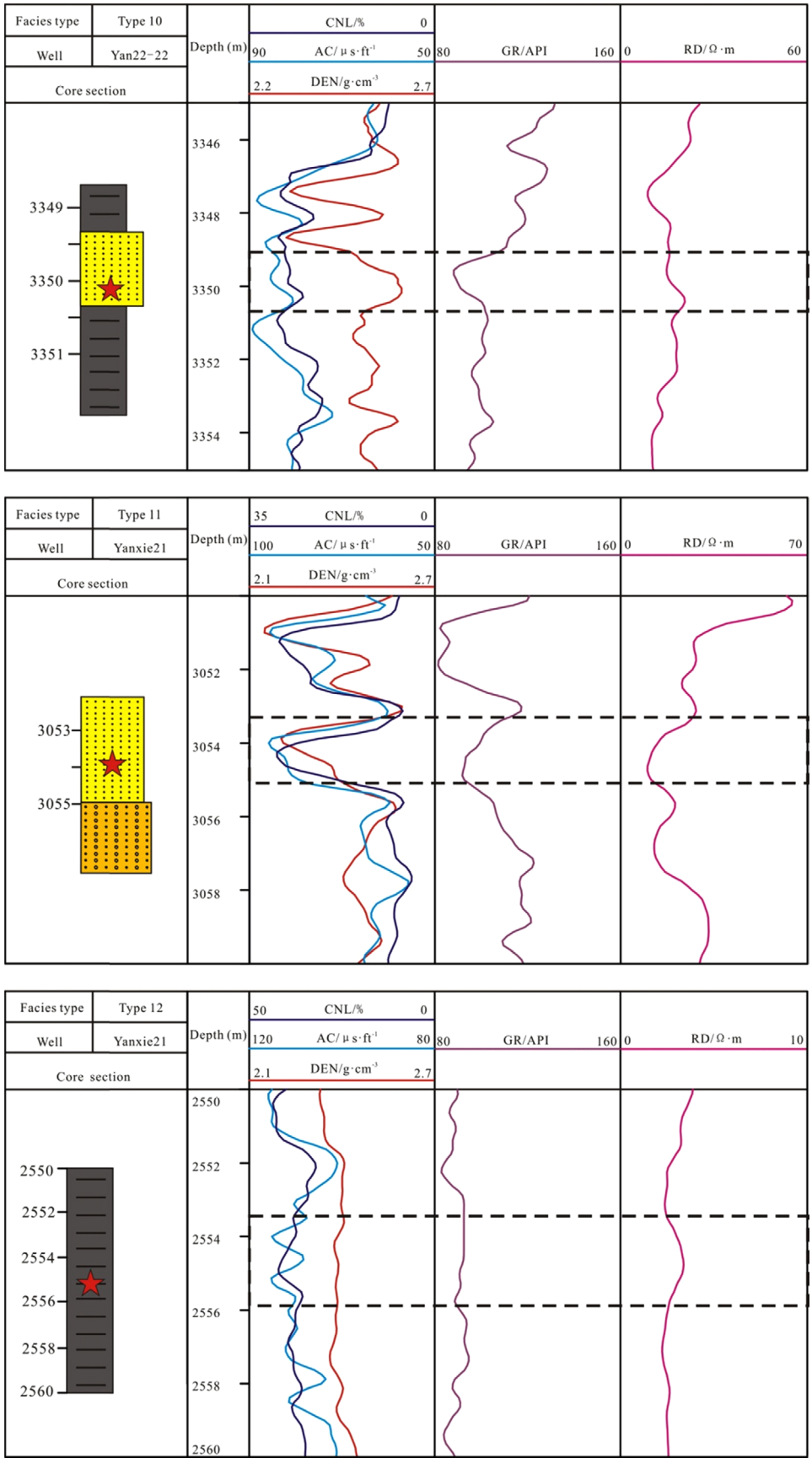

Fig. 5. (continued).

Table 6. Wireline log data of different sedimentary-diagenetic facies in the Eocene Es4 interval

Sedimentary-diagenetic facies	DEN (g/cm^{-3})	AC (μs/ft)	CNL (%)	GR (API)	RD (Ω·m)
Type 1	High value (2.57–2.68)	Low value (55.6–61.1)	Low value (1.33–7.22)	High value (143.4–171.2)	High value (57.9–94.7)
Type 2	High value (2.60–2.68)	Low value (55.8–63.4)	Low value (8.42–12.62)	Medium to high value (108.8–119.8)	High value (41.8–85.6)
Type 3	Medium to high value (2.48–2.65)	Low to medium value (58.0–72.7)	Low value (3.39–8.55)	Medium to high value (112.7–128.6)	Medium value (41.9–60.7)
Type 4	Medium to high value (2.55–2.60)	Low to medium value (59.2–73.4)	Low value (5.58–11.30)	Medium to high value (109.1–122.2)	Medium value (26.8–42.2)
Type 5	Medium value (2.44–2.52)	Medium value (67.8–80.4)	Medium value (10.53–15.88)	Medium to high value (102.3–136.2)	Low to medium value (11.9–38.4)
Type 6	Medium to high value (2.54–2.65)	Low value (57.6–62.2)	Low value (5.31–7.27)	Medium to high value (114.8–139.6)	Medium value (28.7–48.4)
Type 7	Medium-high (2.45–2.55)	Medium-low (63.9–78.6)	Medium (8.92–11.40)	Medium (113.2–130.5)	Medium-low (20.7–31.7)
Type 8	Low to medium value (2.23–2.48)	Medium value (74.8–90.4)	Medium to high value (14.14–35.84)	Low to medium value (80.6–115.3)	Low value (5.1–16.9)
Type 9	Medium value (2.54–2.68)	Low value (55.3–62.9)	Medium value (7.89–12.29)	Low to medium value (83.8–108.4)	Medium to high value (31.1–69.2)
Type 10	Medium value (2.45–2.61)	Medium to high value (78.3–89.1)	Medium to high value (18.13–25.50)	Low value (82.5–103.1)	Low to medium value (16.8–30.9)
Type 11	Low to medium value (2.21–2.51)	High value (79.9–94.8)	High value (18.44–29.80)	Low value (84.9–99.3)	Low value (10.1–19.6)
Type 12	Low value (2.33–2.45)	High value (95.1–113.9)	High value (27.76–40.56)	Low value (69.9–85.7)	Low value (2.4–3.9)

these facies and it allows us to conduct log identification of sedimentary-diagenetic facies based on conventional wireline logs. In this study, the workflow to identify sedimentary-diagenetic facies involves the following aspects: (1) determine the real types of sedimentary-diagenetic facies based on core and thin section petrography; (2) collect corresponding log data of the specific sedimentary-diagenetic facies; (3) accomplish Bayes discriminant analysis of combined wireline logs by SPSS software to identify sedimentary-diagenetic facies; (4) compare the predicted sedimentary-diagenetic types with the real results and conduct cross-plot analysis of log data to improve the accuracy of the predicted identification results.

5.1.1. Bayes discriminant analysis (BDA)

Wireline log data (including DEN, AC, CNL, GR and RLLD data) from twelve sedimentary-diagenetic facies were collected and these log data from different facies can be relatively well separated by two typical Bayes discriminant functions. Subsequently, the corresponding Bayes discriminant functions of these twelve facies were obtained by the SPSS software and expressed as below:

$$\text{Type 1: } Y1 = 24.99*AC - 3.33*CNL + 2114.5*DEN + 5.01*GR + 0.59*RLLD - 3892.11, \quad (8)$$

$$\text{Type 2: } Y2 = 24.93*AC - 3.30*CNL + 2096.9*DEN + 4.51*GR + 0.5*RLLD - 3770.11, \quad (9)$$

$$\text{Type 3: } Y3 = 25.62*AC - 3.90*CNL + 2096.3*DEN + 4.47*GR + 0.31*RLLD - 3793.72, \quad (10)$$

$$\text{Type 4: } Y4 = 25.75*AC - 3.94*CNL + 2090.2*DEN + 4.49*GR + 0.51*RLLD - 3796.91, \quad (11)$$

$$\text{Type 5: } Y5 = 25.95*AC - 3.89*CNL + 2083.8*DEN + 4.50*GR + 0.26*RLLD - 3786.90, \quad (12)$$

$$\text{Type 6: } Y6 = 24.99*AC - 3.57*CNL + 2087.3*DEN + 4.68*GR + 0.31*RLLD - 3757.23, \quad (13)$$

$$\text{Type 7: } Y7 = 25.47*AC - 3.80*CNL + 2072.8*DEN + 4.53*GR + 0.23*RLLD - 3729.59, \quad (14)$$

$$\text{Type 8: } Y8 = 25.94*AC - 3.83*CNL + 2028.8*DEN + 4.15*GR + 0.18*RLLD - 3614.84, \quad (15)$$

$$\text{Type 9: } Y9 = 24.70*AC - 3.46*CNL + 2063.6*DEN + 4.22*GR + 0.48*RLLD - 3636.19, \quad (16)$$

$$\text{Type 10: } Y10 = 27.2*AC - 4.02*CNL + 2143.7*DEN + 4.28*GR + 0.30*RLLD - 4011.67, \quad (17)$$

$$\text{Type 11: } Y11 = 26.9*AC - 4.07*CNL + 2067.6*DEN + 4.14*GR + 0.22*RLLD - 3782.10, \quad (18)$$

$$\text{Type 12: } Y12 = 28.3*AC - 4.22*CNL + 2168.2*DEN + 4.30*GR + 0.21*RLLD - 4167.99. \quad (19)$$

The sedimentary-diagenetic facies can be identified based on the principle of the maximum posterior probability of the Bayes discriminant analysis (BDA). The discriminant accuracy of these twelve types of sedimentary-diagenetic facies is summarized in

https://doi.org/10.1007/s12303-018-0058-4

Table 7. Discriminant probabilities of the 12 types of sedimentary-diagenetic facies in the Eocene Es4 interval

Real type	BDA predicted type												
	Type 1	Type 2	Type 3	Type 4	Type 5	Type 6	Type 7	Type 8	Type 9	Type 10	Type 11	Type 12	Total
Type 1	100	0.0	0.0	0.0	0.0	0.0	0.0	0.0	0.0	0.0	0.0	0.0	100
Type 2	0.0	85	0.0	0.0	0.0	15	0.0	0.0	0.0	0.0	0.0	0.0	100
Type 3	0.0	0.0	11.9	17.6	17.6	52.9	0.0	0.0	0.0	0.0	0.0	0.0	100
Type 4	0.0	37.5	0.0	62.5	0.0	0.0	0.0	0.0	0.0	0.0	0.0	0.0	100
Type 5	0.0	0.0	0.0	0.0	83.3	0.0	16.7	0.0	0.0	0.0	0.0	0.0	100
Type 6	0.0	6.7	0.0	0.0	0.0	93.3	0.0	0.0	0.0	0.0	0.0	0.0	100
Type 7	0.0	0.0	0.0	0.0	23.1	0.0	76.9	0.0	0.0	0.0	0.0	0.0	100
Type 8	0.0	0.0	0.0	0.0	0.0	0.0	0.0	100	0.0	0.0	0.0	0.0	100
Type 9	0.0	0.0	0.0	0.0	0.0	0.0	0.0	0.0	100	0.0	0.0	0.0	100
Type 10	0.0	0.0	0.0	0.0	0.0	0.0	0.0	0.0	0.0	100	0.0	0.0	100
Type 11	0.0	0.0	0.0	0.0	0.0	0.0	0.0	7.1	0.0	14.3	78.6	0.0	100
Type 12	0.0	0.0	0.0	0.0	0.0	0.0	0.0	0.0	0.0	0.0	0.0	100	100

Table 7. The results show that the average discriminant accuracy of all the 12 types is 82.6% (Table 7). However, some predicted sedimentary-diagenetic facies have relatively low discriminant accuracies and need to be addressed to improve their predicted accuracy.

5.1.2. Cross plot analysis (CPA)

After wireline log identification of BDA, cross plot analysis (CPA) of wireline logs were another alternative option to identify the specific sedimentary-diagenetic facies that have relatively low discriminant accuracies.

BDA results indicate that the probability for distinguishing the Type 3 as Type 4, Type 5, Type 6 is 17.6%, 17.6%, 52.9%, respectively, and as Type 3 itself is 11.9% (Table 7). The probability for distinguishing the Type 4 as Type 4 itself and Type 2 is 62.5% and 37.5%, respectively (Table 7). The probability for distinguishing the Type 7 as Type 7 itself and Type 5 is 76.9% and 23.1%, respectively (Table 7). The probability for distinguishing the Type 11 as Type 8, Type 10 is 7.1%, 14.3%, and as Type 11 itself is 78.6%.

Cross-plots of AC versus GR, AC versus CNL, GR versus RD are successively used to identify Type 6, Type 2, Type 3 and Type 4 facies, respectively (Figs. 6a–c). In addition, the value range of wireline logs (AC, CNL, GR and RD) can be used to distinguish Type 2, Type 3, Type 4 and Type 6 facies (Table 8). Cross-plots of CNL versus DEN, AC versus CNL are successively used to identify Type 4, Type 5 and Type 7 facies, respectively (Figs. 6d and e). Moreover, the value range of wireline logs (DEN, CNL, AC) can be also used to distinguish Type 4, Type 5 and Type 7 facies (Table 8). Cross-plots of CNL versus RD are used to identify Type 10 and Type 11 facies (Fig. 6f). The value range of wireline logs (CNL, RD) can be used to distinguish Type 10 and Type 11 facies (Table 8).

Compare the predicted discriminant results with the real types (Table 9), the total accuracy improves significantly and ranges from 82.4% to 100% with an average of 94.7% based on back evaluation of the database through the Bayes discriminant and the cross-plots analysis.

5.2. Reservoir Porosity and Permeability of Sedimentary-Diagenetic Facies

As discussed above, the reservoir quality is largely controlled by both sedimentary lithofacies and diagenetic facies, therefore, the reservoir porosity and permeability can be precisely confined and predicted by specific sedimentary-diagenetic facies (e.g., Lai et al., 2018). Cross-plots of reservoir quality versus burial depth for 11 sedimentary-diagenetic facies indicate that the variation range of reservoir porosity and permeability of specific sedimentary-diagenetic facies is relatively narrow, with ±2% for porosity and $\pm 1 \times 10^{-3}$ μm^2 for permeability (Fig. 7).

The reservoir porosity and permeability for compaction-dominant facies (Type 1, 2, 3, 6, 9; Fig. 7) show a progressively decrease trend with burial depth as a result of increase compaction with depth. The reservoir porosity and permeability for cementation-dominant facies (Type 4, 7, 10; Fig. 7) show a relatively steady tread with burial depth due to extensive cementation occurring prior to significant compaction. The reservoir porosity and permeability for dissolution-dominant facies (Type 8, 11; Fig. 7) show a gradually decreasing trend with depth due to compaction but also show some increase with depth due to strong dissolution. Based on the variation of reservoir porosity and permeability of sedimentary-diagenetic facies with depth, the vertical evolution of reservoir quality with depth in the Eocene Es4 interval can be precisely predicted.

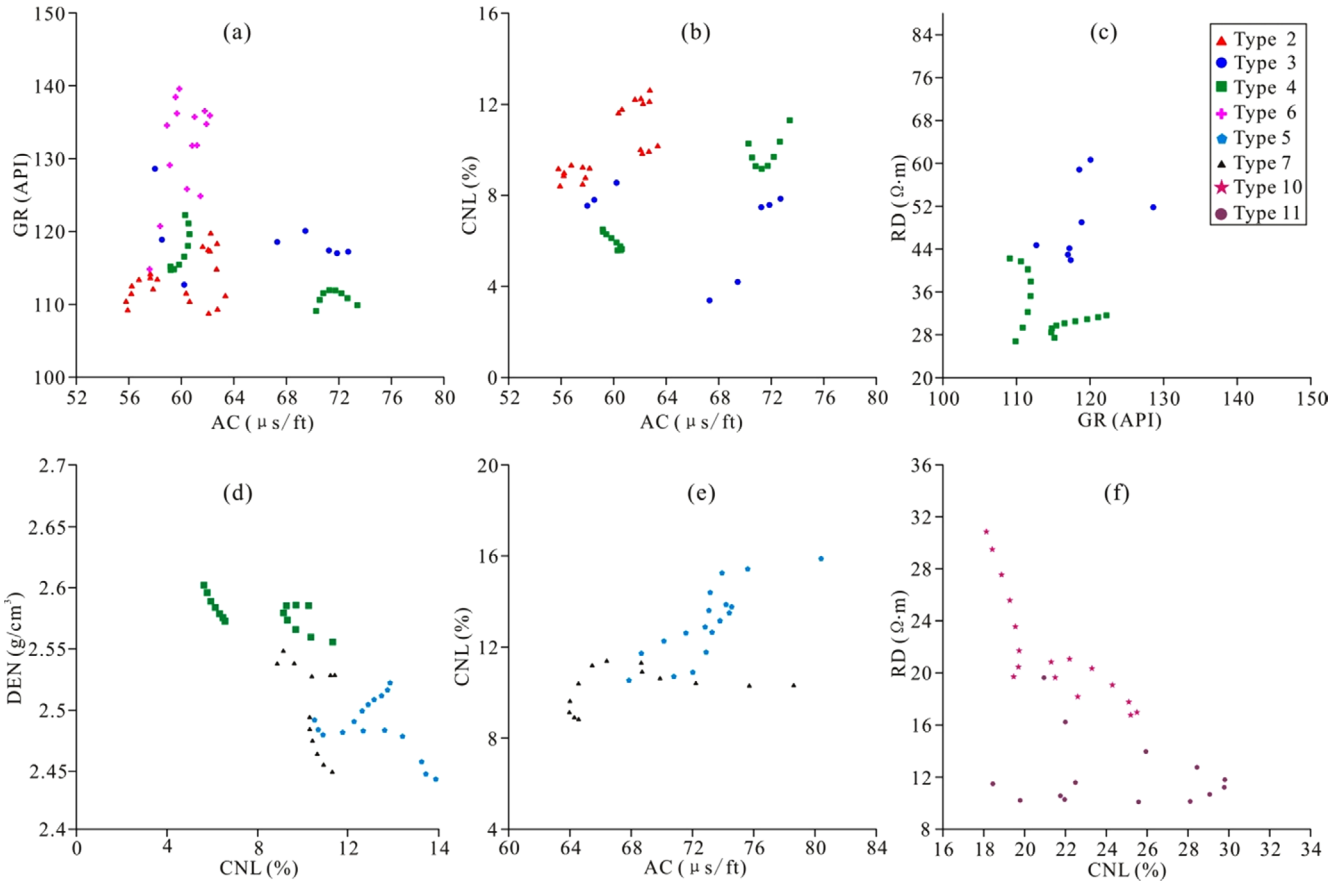

Fig. 6. (a–c): Cross-plot discriminant analysis of Type 2, Type 3, Type 4 and Type 6 facies; (d and e): Cross-plot discriminant analysis of Type 4, Type 5 and Type 7 facies; (f) Cross-plot discriminant analysis of Type 10 and Type 11 facies.

Table 8. Log data range of different types of facies in the Eocene Es4 interval

Facies types	AC (μs/ft)	CNL (%)	GR (API)	RD (Ω.m)	DEN (g/cm^3)
Type 2	55.8~63.4	8.42~12.62	108.8~119.8	41.8~85.6	–
Type 3	58.0~72.7	3.39~8.55	112.7~128.6	41.9~60.7	–
Type 4	59.2~73.4	5.58~11.30	109.1~122.2	26.8~42.2	2.55~2.60
Type 6	57.6~62.2	5.31~7.27	114.8~139.6	28.7~48.4	–
Type 5	67.8~80.4	10.53~15.88	–	–	2.44~2.52
Type 7	63.9~78.6	8.82~11.40	–	–	2.45~2.55
Type 10	–	18.13~25.50	–	16.8~30.9	–
Type 11	–	18.44~29.80	–	10.1~16.8	–

5.3. Distribution of Reservoir Porosity and Permeability

Based on wireline log identification of sedimentary-diagenetic facies, the sedimentary-diagenetic facies of single borehole can be predicted. Some thin-bedded facies are integrated and combined into thick-bedded, predominant facies types (Fig. 8). Cross-section of sedimentary-diagenetic facies in the Eocene Es4 interval shows that dissolution-dominant facies (Type 5, 8, 11; Fig. 8) are mainly developed in the central sections of thick-bedded sandbody, compaction-dominant facies (Type 3, 6; Fig. 8) mainly developed in the bottom of thick-bedded sandbody, and cementation-dominant facies (Type 4, 7, 10; Fig. 8) mainly developed in the margin of thick-bedded sandbody which are adjacent to mudstones.

Using the cross-plots of reservoir porosity and permeability versus burial depth of the sedimentary-diagenetic facies (Fig. 7), the distribution of reservoir porosity and permeability can be quantitatively predicted (Figs. 9 and 10) based on the distribution of sedimentary-diagenetic facies (Fig. 8). The results show that high zones of porosity and permeability mainly distributed in

https://doi.org/10.1007/s12303-018-0058-4

Table 9. The total predicted accuracy for 12 types of sedimentary-diagenetic facies after Bayes discriminant and cross-plot analysis

Real type	Predicted discriminant type												
	Type 1	Type 2	Type 3	Type 4	Type 5	Type 6	Type 7	Type 8	Type 9	Type 10	Type 11	Type 12	Total
Type 1	100	0.0	0.0	0.0	0.0	0.0	0.0	0.0	0.0	0.0	0.0	0.0	100
Type 2	0.0	95	0.0	0.0	0.0	5	0.0	0.0	0.0	0.0	0.0	0.0	100
Type 3	0.0	0.0	82.4	5.8	0.0	11.8	0.0	0.0	0.0	0.0	0.0	0.0	100
Type 4	0.0	12.5	0.0	87.5	0.0	0.0	0.0	0.0	0.0	0.0	0.0	0.0	100
Type 5	0.0	0.0	0.0	0.0	94.4	0.0	5.6	0.0	0.0	0.0	0.0	0.0	100
Type 6	0.0	0.0	0.0	0.0	0.0	100	0.0	0.0	0.0	0.0	0.0	0.0	100
Type 7	0.0	0.0	0.0	0.0	7.7	0.0	92.3	0.0	0.0	0.0	0.0	0.0	100
Type 8	0.0	0.0	0.0	0.0	0.0	0.0	0.0	100	0.0	0.0	0.0	0.0	100
Type 9	0.0	0.0	0.0	0.0	0.0	0.0	0.0	0.0	100	0.0	0.0	0.0	100
Type 10	0.0	0.0	0.0	0.0	0.0	0.0	0.0	0.0	0.0	100	0.0	0.0	100
Type 11	0.0	0.0	0.0	0.0	0.0	0.0	0.0	0.0	0.0	14.3	85.7	0.0	100
Type 12	0.0	0.0	0.0	0.0	0.0	0.0	0.0	0.0	0.0	0.0	0.0	100	100

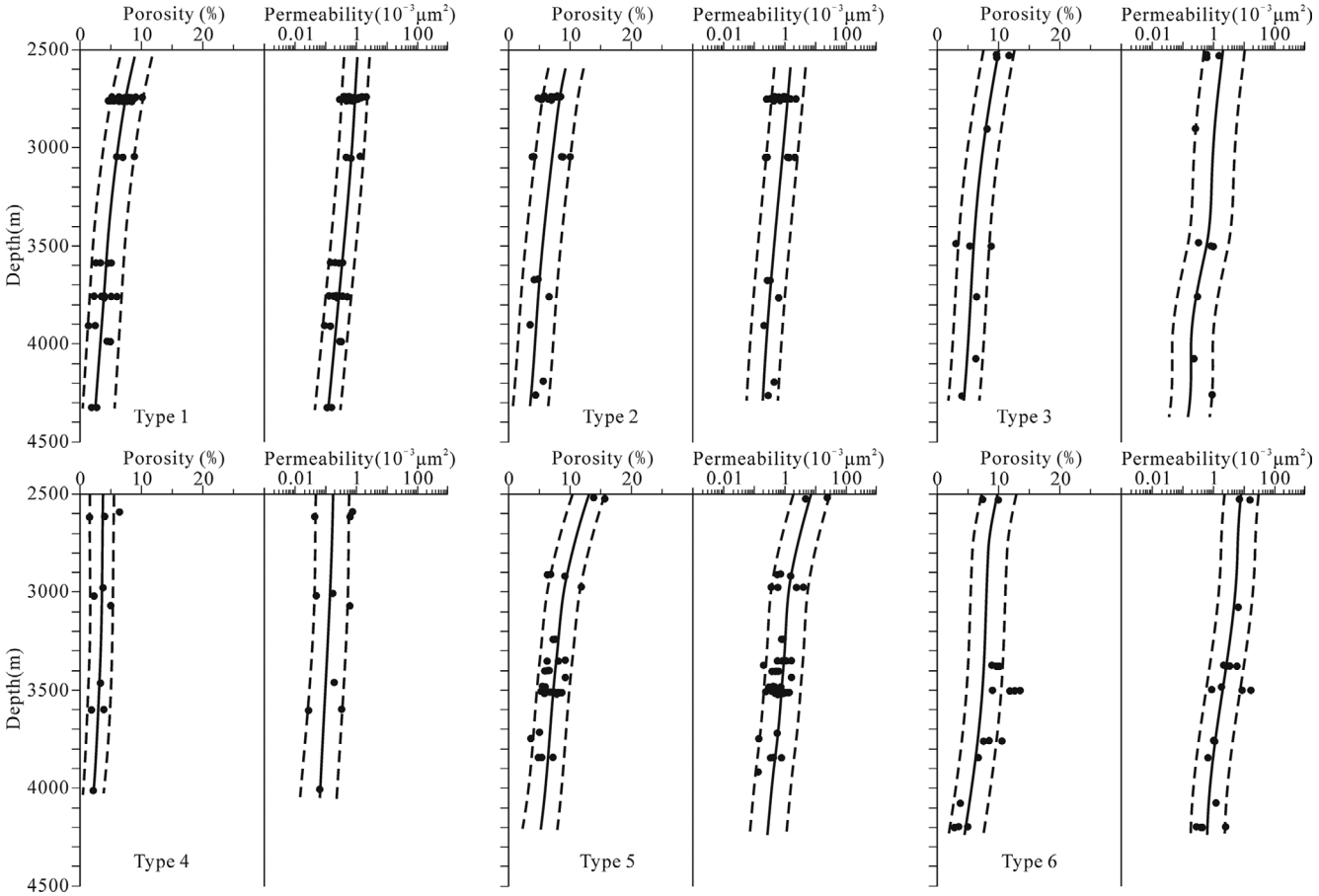

Fig. 7. Plot showing the variation in reservoir porosity and permeability with burial depth of 11 sedimentary-diagenetic facies in the Eocene Es4 interval.

the central sections of thick-bedded sandbody, ranging from 6% to greater than 12% for reservoir porosity and from 1×10^{-3} μm^2 to greater than 6×10^{-3} μm^2 (Figs. 9 and 10). Relatively low zones of porosity (less than 6%) and permeability (less than 1×10^{-3} μm^2) mainly occur in the bottom and the margin of the thick-bedded sandbody (Figs. 9 and 10).

Identification of sedimentary-diagenetic facies associated with conventional wireline logs has important implications for reservoir

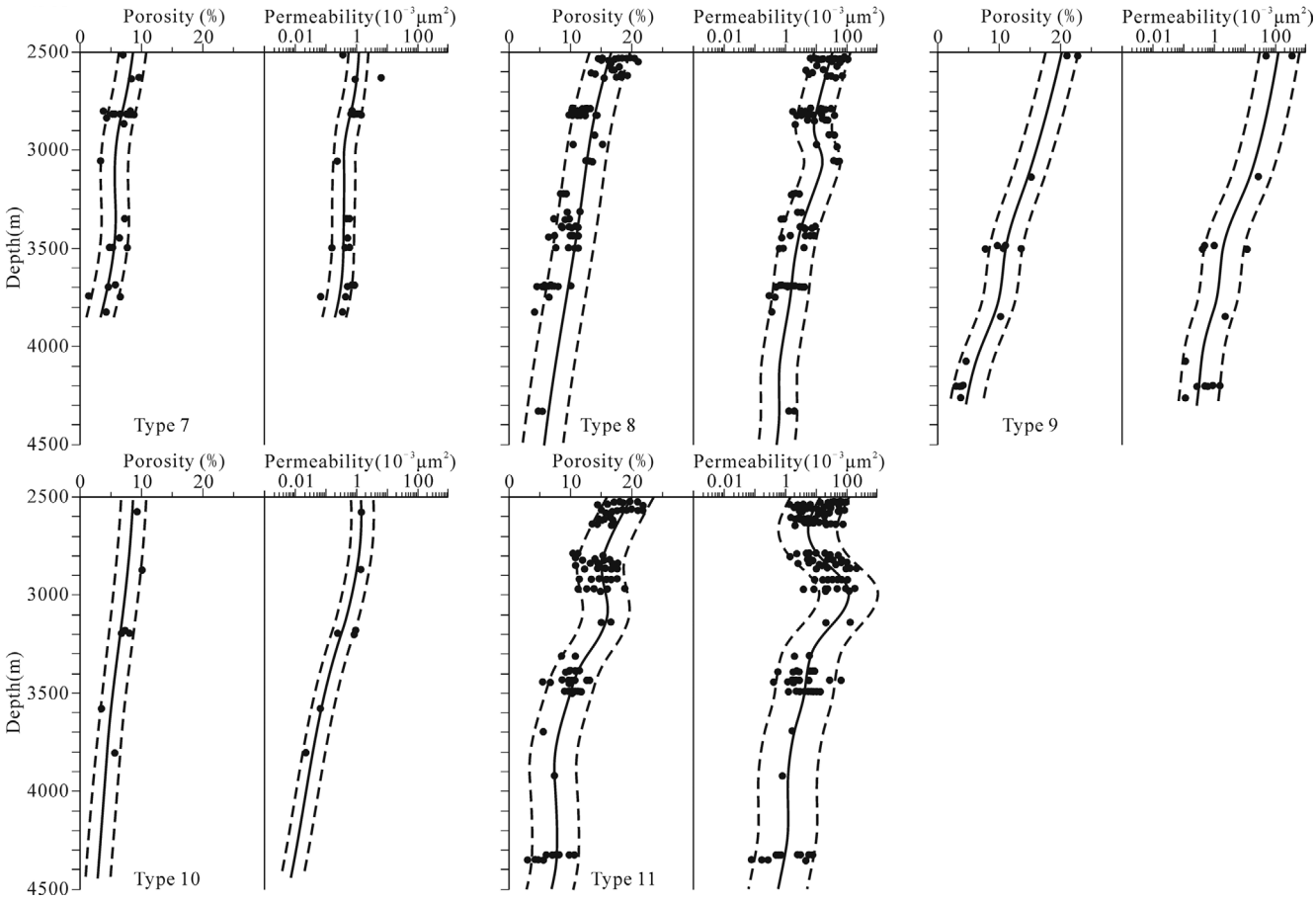

Fig. 7. (continued).

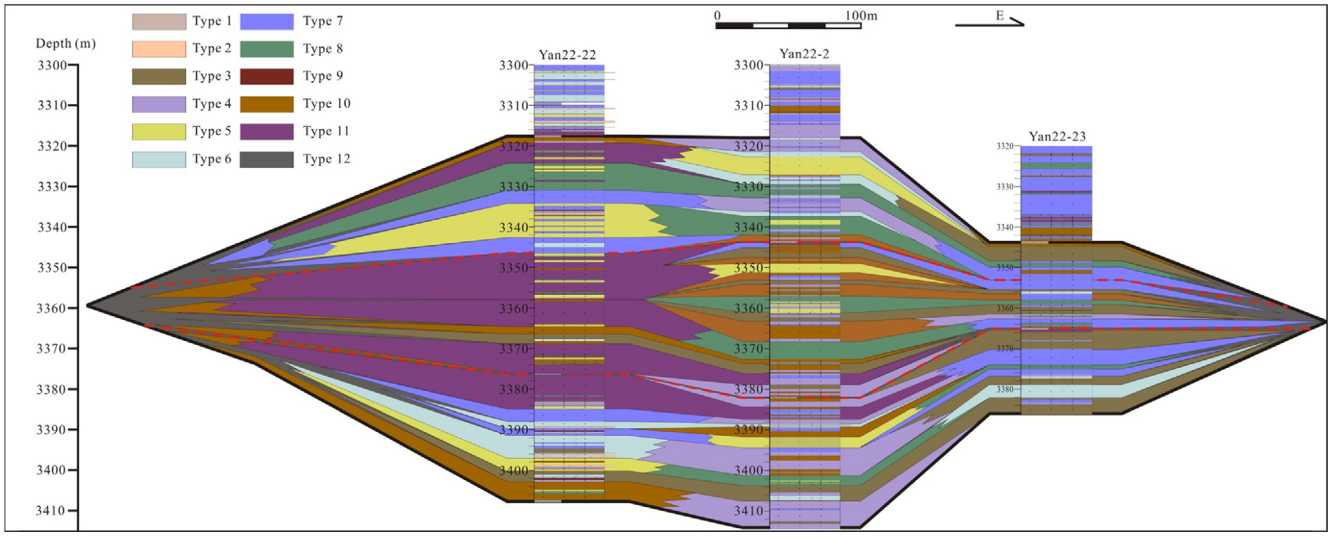

Fig. 8. Cross section showing distribution of sedimentary-diagenetic facies in the Eocene Es4 interval.

quality and wide applications for exploration and development of siliciclastic reservoirs: (1) conventional wireline logs have lower cost than core data to determine depositional and diagenetic information; (2) reservoir porosity and permeability can be more precisely controlled by the sedimentary-diagenetic facies than separate sedimentary lithofacies or diagenetic facies; (3) the spatial distribution of sedimentary-diagenetic facies and related reservoir porosity and permeability can be predicted quantitatively.

https://doi.org/10.1007/s12303-018-0058-4

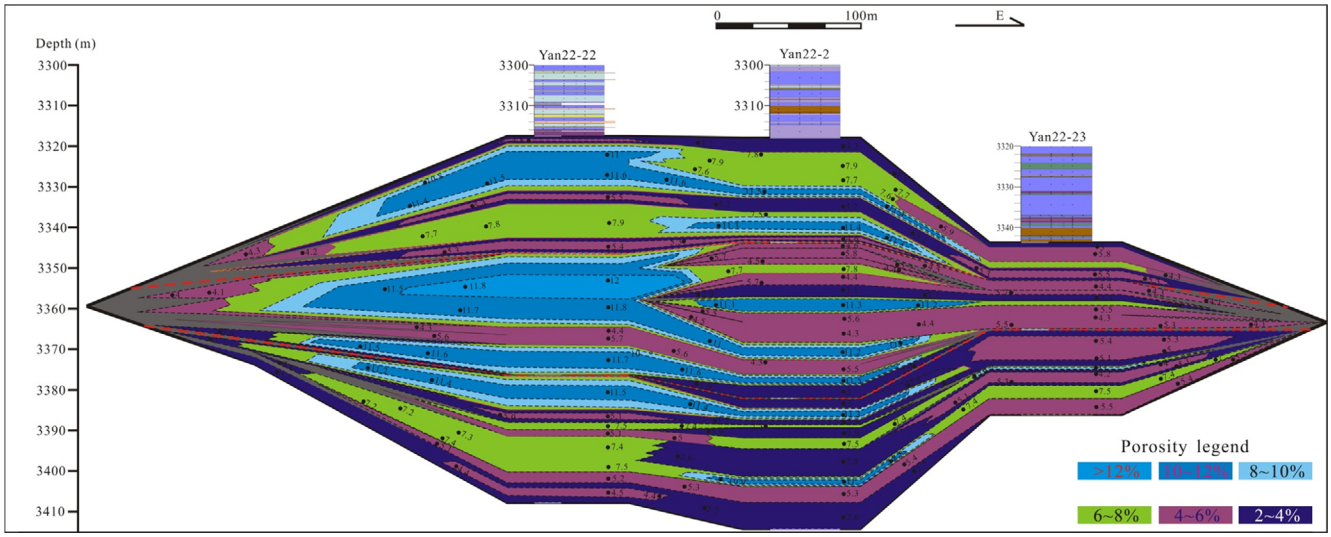

Fig. 9. Spatial distribution of reservoir porosity in the Eocene Es4 interval.

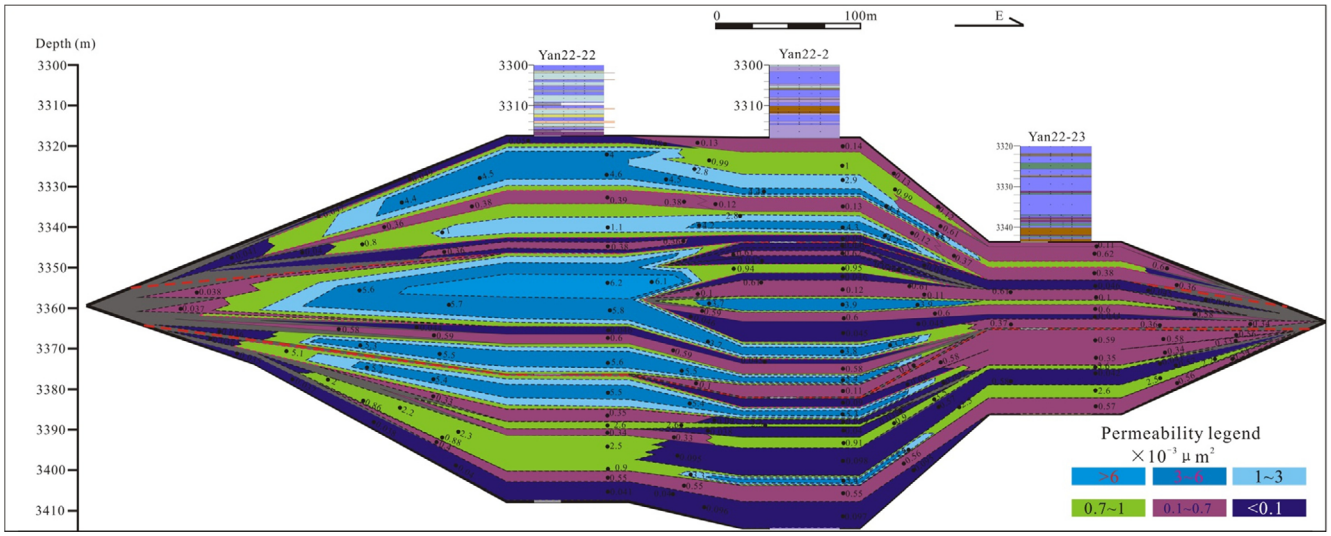

Fig. 10. Spatial distribution of reservoir permeability in the Eocene Es4 interval.

6. CONCLUSIONS

A new facies identification method associated with sedimentary-diagenetic facies is proposed in the Eocene Es4 coarse-grained deposits in the Dongying Depression, Bohai Bay Basin, China. 12 types of sedimentary-diagenetic facies are identified based on core observation, thin section petrography and conventional wireline logs in the Eocene Es4 sandstones. The corresponding reservoir porosity and permeability of these 12 facies with burial depth were determined with the value range of ±2% for porosity and $\pm 1 \times 10^{-3}$ μm^2 for permeability. The spatial distribution of sedimentary-diagenetic facies and related reservoir porosity and permeability can be predicted quantitatively in the Eocene Es4 interval: high zones of porosity and permeability mainly distributed in the central sections of thick-bedded sandbody, with value range from 6% to greater than 12% for reservoir porosity and from 1×10^{-3} μm^2 to greater than 6×10^{-3} μm^2 for reservoir permeability; relatively low zones of porosity (less than 6%) and permeability (less than 1×10^{-3} μm^2) mainly occur in the bottom and the margin of the thick-bedded sandbody. Identification of sedimentary-diagenetic facies associated with conventional wireline logs has important implications for reservoir quality and wide applications for exploration and development of siliciclastic reservoirs.

ACKNOWLEDGMENTS

This research was financially supported by the National Science and Technology Major Special Projects (2016ZX05006-003, 2016ZX05006-007), the National Natural Science Foundation of China (41772137), Shangdong Provincial Natural Science Foundation of China (ZR2017LD005), Foundation in Key

Laboratory of Tectonics and Petroleum Resources (TPR-2017-07), the Natural Science Foundation in Hubei Provence (ZRMS2017000478), the Fundamental Research Funds for the Central Universities (14CX02181A, 17CX05009, 15CX08001A, CUG170630). We would like to thank the Geological Science Research Institute of Shengli Oilfield, SINOPEC for permission to access to the cores. We also thank Dr. Zhukun Wang, Dr. Shaomin Zhang and Dr. Peipei Sun for their help in figure drafting.

REFERENCES

Bjørlykke, K., 2014, Relationships between depositional environments, burial history and rock properties. Some principal aspects of diagenetic process in sedimentary basins. Sedimentary Geology, 301, 1–14.

Cui, Y., Wang, G., Jones, S., Zhou, Z., Ran, Y., Lai, J., Li., R., and Deng, L., 2017, Prediction of diagenetic facies using well logs – a case study from the upper Triassic Yanchang Formation, Ordos Basin, China. Marine and Petroleum Geology, 81, 50–65.

Dickson, J.A., 1965, Carbonate identification and genesis as revealed by staining. Journal of Sedimentary Petrology, 27, 107–118.

Folk, R.L., 1974, Petrology of Sedimentary Rocks. Hemphill Press, Austin, 182 p.

Fu, J., Wu, S., Hu, L., Zhang, H., and Liu, X., 2013, Research on quantitative diagenetic facies of the Yanchang Formation in Longdong Area, Ordos Basin. Earth Science Frontiers, 20, 86–96. (in Chinese with English abstract)

He, J., Ding, W., Jiang, Z., Li, A., Wang, R., and Sun, Y., 2016, Logging identification and characteristic analysis of the lacustrine organic-rich shale lithofacies: a case study from the Es3 shale in the Jiyang Depression, Bohai Bay Basin, Eastern China. Journal of Petroleum Science and Engineering, 145, 238–255.

Jiang, S., Henriksen, S., Wang, H., Lu, Y.C., Ren, J.Y., Cai, D.S., Feng, Y.L., and Weimer, P., 2013, Sequence-stratigraphic architectures and sand-body distribution in Cenozoic rifted lacustrine basins, east China. American Association of Petroleum Geologists Bulletin, 97, 1447–1475.

Lai, J., Wang, G., Chai, Y., Ran, Y., and Zhang, X., 2015, Depositional and diagenetic controls on reservoir pore structure of tight gas sandstones: evidence from Lower Cretaceous Bashijiqike Formation in Kelasu Thrust Belts, Kuqa Depression in Tarim Basin of West China. Resource Geology, 65, 55–75.

Lai, J., Wang, G., Chai, Y., and Ran, Y., 2016, Prediction of diagenetic facies using well logs: evidences from upper Triassic Yanchang Formation Chang 8 sandstones in Jiyuan Region, Ordos Basin, China. Oil & Gas Science and Technology, 71, 1–23.

Lai, J., Wang, G., Fan, Z., Fan, Z., Chen, J., Wang. S., and Fan, X., 2017, Sedimentary characterization of a braided delta using well logs: the Upper Triassic Xujiahe Formation in Central Sichuan Basin, China. Journal of Petroleum Science and Engineering, 154, 172–193.

Lai, J., Wang, G., Cai, C., Fan, Z., Wang, S., Chen, J., and Luo, G., 2018, Diagenesis and reservoir quality in tight gas sandstones. Geological Journal, 53, 629–646.

Li, Y. and Anderson-Sprecher, R., 2006, Facies identification from well logs: a comparison of discriminant analysis and naïve Bayes classifier. Journal of Petroleum Science and Engineering, 53, 149–157.

Li, J. and Zhou, L., 2008, Respond features of gamma ray log and its application in glutenite of Dongying Depression. Journal of Oil and Gas Technology, 30, 88–91. (in Chinese with English abstract)

Liu, W., Dou, Q., and Huang, S., 2002, Quantitative characterization of diagenesis and diagenetic reservoir facies – a case study of lower member of Jiao 2 block in Kerqin oilfield. Journal of China University of Mining & Technology, 31, 400–403. (in Chinese with English abstract)

Liu, H., Zhao, Y., Luo, Y., Chen, Z., and He, S., 2015, Diagenetic facies controls on pore structure and rock electrical parameters in tight gas sandstone. Journal of Geophysics & Engineering, 12, 587–600.

Lu, G., 2010, Logging comprehensive identification technology of deep sandy conglomerate lithology, Dongying Sag. Well Logging Technology, 34, 169–171. (in Chinese with English abstract)

Ma, B., Eriksson, K., Cao, Y., Jia, Y., Wang, Y., and Gill, B., 2016, Fluid flow and related diagenetic processes in a rift basin: evidence from the Eocene Es4 interval, Dongying Depression, Bohai Bay Basin, China. American Association of Petroleum Geologists Bulletin, 100, 1633–1662.

Ma, B., Cao, Y., Eriksson, K., Jia, Y., Wang, Y., and Gill, B., 2017, Depositional and diagenetic controls on deeply-buried Eocene sublacustrine fan reservoirs in the Dongying Depression, Bohai Bay Basin, China. Marine and Petroleum Geology, 82, 297–317.

Ozkan, A., Cumella, S.P., Milliken, K.L., and Laubach, S.E., 2011, Prediction of lithofacies and reservoir quality using well logs, late cretaceous williams fork formation, mamm creek field, Piceance basin, Colorado. American Association of Petroleum Geologists Bulletin, 95, 1699–1723.

Rahman, M.J. and McCann, T., 2012, Diagenetic history of the Surma Group sandstones (Miocene) in the Surma Basin, Bangladesh. Journal of Asian Earth Sciences, 45, 65–78.

Wang, Y., Cao, Y., Ma, B., Liu, H., Gao, Y., and Chen, L., 2014, Mechanism of diagenetic trap formation in nearshore subaqueous fans on steep rift lacustrine basin slopes – a case study from the Shahejie Formation on the north slope of the Minfeng Subsag, Bohai Basin, China. Petroleum Sciences, 11, 481–494.

Wang, Y., Cao, Y., and Xi, K., 2013, A recovery method for porosity evolution of clastic reservoirs with geological time:a case study from the upper submember of Es4 in the Dongying Depression, Jiyang Subbasin. Acta Petrolei Sinica, 34, 1100–1110. (in Chinese with English abstract)

Xu, C., Cronin, T.P., McGinness, T.E., and Steer, B., 2009, Middle Atokan sediment gravity flows in the Red Oak field, Arkoma Basin, Oklahoma: a sedimentary analysis using electrical borehole images and wireline logs. American Association of Petroleum Geologists Bulletin, 93, 1–29.

Zhang, X., Zou, C., and Tao, S., 2009, Diagenetic facies types and semi-quantitative evaluation of low porosity and permeability sandstone of the fourth member Xujiahe Formation, Guangan Area, Sichuan Basin. Acta Sedimentologica Sinica, 28, 50–56. (in Chinese with English abstract)

Zou, C., Tao, S., and Zhou, H., 2008, Genesis, classification and evaluation method of diagenetic facies. Petroleum Exploration and Development, 35, 526–540.

https://doi.org/10.1007/s12303-018-0058-4